A New Constitutive Model for the Chemical Aging of Rubber Networks in Deformed States

Joanne Budzien,*,† Dana R. Rottach,‡ John G. Curro,† Chi S. Lo,† and Aidan P. Thompson†

Sandia National Laboratories, Albuquerque, New Mexico 87185, and Department of Chemical and Nuclear Engineering, University of New Mexico, Albuquerque New Mexico 87106

Received June 18, 2008; Revised Manuscript Received October 26, 2008

ABSTRACT: This paper describes the finite element implementation of a recently developed constitutive model for the chemical aging of rubber in deformed states. The model was developed from molecular dynamics simulations that investigated two stage networks. The model includes the effects of multiple stages of cross-linking and scission while the sample is deformed and the effects of physical entanglements. Given the deformation and chemical history of a sample, finite element calculations using this model are shown to make quantitative predictions of permanent set for two sample experimental systems.

I. Introduction

Rubbers are widely used materials for a variety of applications. However, they are not inert materials and, frequently, time-dependent changes in mechanical properties are an important concern. Much experimental work[1] has been performed on aging samples to investigate those changes. This aging of the material may be the result of many processes that are generally categorized into two types:[2−4] physical and chemical. Physical aging is the movement of the polymer chains with no modification to the networks while chemical aging involves reactions that change the network topology of the sample.

Both of these kinds of aging contribute to the reduction of stress during relaxation experiments. The proportion of physical to chemical aging varies by rubber formulation. In this paper, we consider only chemical aging because that is the dominant effect at high temperature or long time. Thus, to make comparisons with experiment, we have chosen two systems that have primarily chemical aging occurring.

The evidence for only a small effect of physical aging appears in the permanent set data for both systems. The uniaxial extension data is from the classic study by Andrews, Tobolsky, and Hanson.[5] We compare with the butyl gum, which was found to change from a permanent set of 42.9% to 42.3% over the course of a week during an investigation on the effect of waiting time between measurements on permanent set. If physical aging were a significant factor, the change in permanent set with waiting time would be appreciable. Thus, we assume that little error occurs in attributing the entire stress relaxation to chemical aging.

The compression data is from the experiments of Gillen, Celina, and Bernstein,[6] where the expressed purpose was to compare accelerated aging experiments with field-aged samples, and therefore, great care was taken to obtain permanent set values that were free from physical aging effects. We use the highest temperature data set from that paper, which are the force measurements that are the least likely to contain significant physical aging. The fact that our permanent set predictions are close to the experimentally determined permanent set shows that our assumption of minimal physical relaxation in the high temperature data set is acceptable.

The chemical aging of the polymer networks is often neglected in constitutive models for rubber. While Tobolsky proposed the independent network hypothesis[5] in the 1940s, only a few constitutive models have been built on it. Wineman and Rajagopal[7] published the framework for a constitutive model that included multiple stages of cross-linking and scission. That model was extended by Shaw, Jones, and Wineman[8] to include the effects of physical aging and nonhomogeneous reactions. However, most of the work published using that model does not actually use the multiple networks to compare with experiment. The notable exception is section 5.10 in Jones' dissertation,[9] where multiple stages were used to parametrize the model and then shown to be a good fit to the data for similar experiments.

Another constitutive model that successfully builds on the independent network hypothesis is due to Septanika and Ernst.[10] Once fitted to the experimental stress relaxation experiments, the resulting parametrization makes good predictions for the time-dependent stretches in creep experiments and the time-dependent Poisson's ratio.

However, both those models neglect two important points: the trapped physical entanglements form another network, which can also support stress, and, in many cases, the "independent" networks proposed by Tobolsky cannot be truly independent. Both of those points were published in the open literature in the middle of the twentieth century,[11,12] and recent simulations[13−15] have shown that those points are important if one wants to parametrize models starting from the underlying chemistry instead of relying on fits to experimental data. The constitutive model presented here draws on the results of those simulations to include not only the scission and cross-linking of multiple networks under strain, but also the necessary interplay between the "independent" networks and the contribution of the entanglement network to the stress. To demonstrate the effectiveness of the model, we have implemented it into a finite element code, parametrized it using experimental stress relaxation data, and then predicted permanent set in good agreement with experimental data.

A brief recap of rubber elasticity is in order. Rubber supports stress because of its network structure. Seals and other rubber items are often put into service in a deformed state. However, these components are not inert, and chemical reactions occur while the components are in service. Any given reaction is local

* Author to whom correspondence should be addressed. E-mail: jlbudzi@sandia.gov.
† Sandia National Laboratories.
‡ Department of Chemical and Nuclear Engineering, University of New Mexico. Present address: Abratech Corporation, Ste. 213, 475 Gate 5 Rd, Sausalito, CA 94965.

10.1021/ma801373z CCC: $40.75
Published on Web 11/21/2008

and rapid. While a single reaction has an insignificant effect on the properties of a material, the cumulative effect of these reactions can cause enormous changes in the mechanical properties of a sample.

For example, cross-linking in a strained state forms a second network. A network that is in the deformation state at which it was formed has zero stress. This deformation is termed the state of ease for that network. The Tobolsky independent network model[5] states that the effects of the two networks are additive. Therefore, merely cross-linking the sample to form a second network has little effect as long as the sample remains in that deformed state. Chemically, the cross-links in the two networks may be identical. The difference is the state of strain in which they were introduced. In spite of making little change in the sample properties when introduced, this second network can have a large effect if the sample is then further deformed. Indeed, simply releasing the sample will show the presence of a second network. The failure of a sample to return to its original shape is a measure of the relative strength of the two networks and can be quantified through the measurement of permanent set. Simulations[13] have confirmed the additive aspect of the independent network hypothesis.

If the original network scissions, the situation becomes more complicated. The second network forms subject to topological restrictions imposed by the original network. Therefore, scission of the first network does not eliminate its effect on the stress state of the sample. The sample retains a memory of cross-linking and strain history because a certain percentage of the second network cross-links will act as though they were first stage cross-links. Physically, this is not a one-for-one exchange of cross-link identities, but rather the result of the bias in the cross-linking of the second network. Flory[12] and Fricker[16] both addressed this complication mathematically through stress transfer functions and effective networks. The stress transfer function quantifies what percentage of each set of cross-links is acting as which network. The independent network model can then be applied using an effective network cross-link density, which is calculated from the actual cross-link density modified by the stress transfer function.

In previous work, molecular dynamics simulations[14,15] of coarse-grained polymer networks reacting under deformation were performed to investigate the change in stress with chemical reaction. Those simulations have shown the effective network formulation to be a reasonable approach for chemical aging.[14,15] On the basis of those simulations, we proposed a constitutive model that incorporates the effects of multiple stages of cross-linking and scission by using a stress transfer function. This use of the stress transfer function is a differentiating feature of our constitutive model. Our simulations have also shown the effect of trapped physical entanglements acting as another network and our constitutive model includes those effects. Section II of this paper describes the resulting constitutive model. We have implemented this constitutive model into the Sandia-proprietary finite element code Adagio.[17] This constitutive model was developed from the physics of the network shown by simulation. By taking chemistry from experimental stress relaxation data, we have quantitatively predicted permanent set in agreement with experiment. Section III shows the results of the finite element calculations and compares with two experimental data sets, one for compression and one for extension. Section IV concludes the paper with a brief summary and future directions.

II. Theory

A. Constitutive Model. Our simulations have shown[14,15] that a sum of contributions from both the chemical cross-links and the physical entanglements (adequately captured by the slip-tube model) determine the stress. The simulations were performed at constant volume, in keeping with the standard assumption that rubber is incompressible. However, finite element calculations have difficulty converging with incompressible materials. Therefore, a modification to the constitutive model to allow for an augmented Lagrangian approach was employed. This augmented Lagrangian approach is an iterative procedure that uses a compressible material as an initial guess and then solves for progressively stiffer materials until the desired material is obtained. The total stress $\boldsymbol{\sigma}$ can be written as the sum of three terms corresponding to the chemical cross-links, the physical entanglements, and a volume term:

$$\boldsymbol{\sigma} = \boldsymbol{\sigma}_{chemical} + \boldsymbol{\sigma}_{physical} + \boldsymbol{\sigma}_{volume} \tag{1}$$

Each of these terms is discussed in this section. The phantom chain model was modified to use effective cross-link densities with the stress transfer function. A brief discussion of the stress transfer function and effective networks is given in the first subsection. The second subsection discusses modifications to the slip-tube model. As originally formulated, the free energy calculation for the slip-tube model[18] involves a self-consistent calculation at every deformation. This is computationally intensive and impractical for large systems using the finite element code. Instead, a deformation range suitable for O-rings has been identified and self-consistent calculations were done within that range. The resulting strain energy was fit analytically to a power series of strain invariants. The method used to determine that power series is given in the second subsection along with the coefficients of the power series and figures illustrating goodness of fit. The third subsection shows the complete constitutive equation.

B. The Phantom Chain Model and Effective Networks. The Cauchy stress for the phantom chain model can be written as

$$\boldsymbol{\sigma} = \frac{G}{\det(\boldsymbol{\lambda})}\boldsymbol{\lambda}\boldsymbol{\lambda}^T + p\boldsymbol{I} \tag{2}$$

where G is a modulus related to the cross-link density, $\boldsymbol{\lambda}$ is the deformation gradient tensor, and p is an indeterminate Lagrangian multiplier related to the hydrostatic pressure. However, this equation is valid only for a single network that experiences no further chemical reactions. During chemical aging, cross-linking and scission may happen while the sample is deformed. Cross-linking while in a strained state leads to another network being created. Multiple stages of deformation with cross-linking at each stage will create multiple networks. According to the independent network model, each network will have a state of ease (zero stress state) in the deformation at which it was created. Using the independent network model requires modifying eq 2 to make the deformation relative to the state of ease. Each network i has a stress

$$\boldsymbol{\sigma}_i = \frac{G_i}{\det(\boldsymbol{\lambda})}\boldsymbol{\lambda}\boldsymbol{\lambda}_i^{-1}[\boldsymbol{\lambda}_i^{-1}]^T\boldsymbol{\lambda}^T + p\boldsymbol{I} \tag{3}$$

where $\boldsymbol{\lambda}_i$ is the deformation tensor at which the network i was formed. To obtain the total Cauchy stress, we sum over the contributions from all of the networks:

$$\boldsymbol{\sigma}_{chemical} = \sum_{i=1}^{n} \boldsymbol{\sigma}_i \tag{4}$$

The careful reader will notice that this leads to several terms of $p\mathbf{I}$ being added to the total stress, but since p is not a true hydrostatic pressure, but rather an indeterminate Lagrangian multiplier to ensure that the stress remains zero at the appropriate boundaries, this artificiality of equation construction presents no problems.

Accounting for scission in multiple networks cross-linked in different strain states is more complicated. As an example, cross-link a sample and then stretch it. Cross-link a second time while the sample is held in the stretched deformation. The stress will not change during the cross-linking procedure. Chemically, the cross-links from the two networks are identical; the only difference is the global effect on the stress. Take out all of the original cross-links. The stress will not drop to zero. A portion of the second network acts as though it were the original network with the original state of ease. This phenomenon is a result of the limitations placed on the second network's cross-linking opportunities because of the topology of the original network.

Flory[12] developed a methodology for affine networks that deals with two stages of cross-linking followed by scission of some portion of the original network. The point relevant to this work is the use of a stress transfer function to quantitatively partition cross-link densities into networks based on their effect on the state of ease. Conceptually, the stress transfer function is simple: it defines what fraction of each network assumes the role of an earlier network that has undergone scission. Fricker[16] proposed a simple stress transfer function for phantom networks. Our previous simulation work[15] showed that the Fricker stress transfer function worked for two stage networks. Here, we propose a tractable approximation of that stress transfer function, Φ, for an arbitrary number of networks:

$$\Phi_x^{Rj} = \frac{\text{stage } x \text{ cross-links removed in stage } j}{\text{total number of cross-links added (up through stage } j)} = \frac{G_x^{Rj}}{\sum_{k=1}^{j} G_k^*} \quad (5)$$

The effective network modulus for each network can then be written as

$$G_p^{eff} = G_p\left(1 - \sum_{i=1}^{p-1}\sum_{k=p}^{n} \Phi_i^{Rk}\right) + \sum_{i=p+1}^{n} \Phi_p^{Ri} \sum_{k=p+1}^{i} G_k \quad (6)$$

where the first term is the contribution to earlier stage networks that have lost cross-links and the second term is the contribution from later stage networks because network p underwent scission in a strained state. The total stress calculated from eq 4 will give valid results for systems undergoing cross-linking and scission in strained states, if the effective moduli from eq 6 are used instead of the moduli calculated from the actual cross-linking density for each network.

C. Entanglement Contributions from the Slip-Tube Model. Our previous simulation results[14,15] showed that the entanglement contribution to the stress could be adequately captured by the slip-tube model. While those simulations were done only in uniaxial extension, we assume that the results would be valid for any deformation.

The slip-tube model[18] is a blend of standard slip-link and tube models. The effect of the other chains on a specific chain is modeled by a series of effective slip-links that constitute a deformable tube. While the chain can slip along the tube, the tube is also free to deform anisotropically. In practical terms, this tube deformation mechanism allows the chain to relieve stress by bulging in some directions while being compressed in other directions. The distribution of the chain in three principal directions can be quantified by the $\{g_\alpha\}$, which are scaling factors related to the number of monomers currently in the α direction relative to the original number of monomers in that direction.

The determination of the $\{g_\alpha\}$ is the primary difficulty in calculating the stress from the slip-tube model. The free energy expression is easily expressed in terms of the $\{g_\alpha\}$, but to actually calculate the free energy or the stress requires a self-consistent determination of the $\{g_\alpha\}$ for every deformation. The computational overhead of including this iterative solution for the $\{g_\alpha\}$ in the finite element code is very large. Instead, we have chosen a range of deformations physically reasonable for the possible strain states of a rubber component, performed the self-consistent calculations for a grid of points within those strain states, and fit the resulting strain energy data set to a standard analytic form, which is easily implemented into the finite element code to calculate the stress. This section follows the development of the final stress equation beginning with the original free energy equation continuing through a brief description of the fitting procedure and ending with the resulting expression for the stress.

The free energy expression for the original formulation of the slip-tube model is[18]

$$F = \frac{A}{2}\sum_\alpha \left(\frac{\lambda_\alpha}{g_\alpha^{1/2}} + \frac{g_\alpha^{1/2}}{\lambda_\alpha}\right) - \frac{A}{3}\sum_\alpha \ln\left(\frac{N}{L} g_\alpha\right) \quad (7)$$

where A is an elastic modulus due to the entanglements, λ_α is the principal stretch in the α direction, N is the number of monomers in a chain, and L is the number of effective slip-links per chain. To calculate values for the $\{g_\alpha\}$, eq 7 must be minimized with respect to the $\{g_\alpha\}$ under the condition $\sum_\alpha g_\alpha = 3$. Thus, the $\{g_\alpha\}$ are a function of the $\{\lambda_\alpha\}$.

Solving eq 7 for the $\{g_\alpha\}$ for the general case is difficult, but solving it for a specific deformation is straightforward by formulating the equation in each direction using a Lagrangian multiplier method and solving using the iterative secant method. The resulting equations can be written as:

$$S = g_1 + g_2 + g_3 - 3 \quad (8)$$

$$\frac{12\Lambda}{A} = 3\left(-\frac{\lambda_2}{g_2^{3/2}} + \frac{1}{g_2^{1/2}\lambda_2}\right) - \frac{4}{g_2} \quad (9)$$

$$g_1^{3/2}\left[\frac{12\Lambda}{A}\lambda_1\right] - 3g_1 + 4g_1^{1/2}\lambda_1 + 3\lambda_1^2 = 0 \quad (10)$$

$$g_3^{3/2}\left[\frac{12\Lambda}{A}\lambda_3\right] - 3g_3 + 4g_3^{1/2}\lambda_3 + 3\lambda_3^2 = 0 \quad (11)$$

$$g_2^{1/2}(i+1) = g_2^{1/2}(i) - S(i)\left[\frac{g_2^{1/2}(i) - g_2^{1/2}(i-1)}{S(i) - S(i-1)}\right] \quad (12)$$

where Λ is the Lagrangian multiplier and i is the iteration counter.

We chose $g_2^{1/2}$ as the variable to track through the iterations. Given the deformation state $\{\lambda_\alpha\}$, initial estimates for the $\{g_\alpha\}$, and a first step estimate for g_2, eq 8 can be solved for S and eq 9 can be solved for $12\Lambda/A$. Using that value for $12\Lambda/A$, the cubic equations in $g_\alpha^{1/2}$ for the other two directions are solved. In every case, the physical root (i.e., positive and smaller than $\sqrt{3}$) is chosen. The iterations continue until either $S(i) = S(i-1)$ or $g_2^{1/2}(i) = g_2^{1/2}(i-1)$.

For use with the finite element code, an analytic strain energy function is needed for arbitrary deformation. The analytic strain energy function chosen was the standard form for incompressible materials written as a sum of invariants[19] for strain energy W:

$$W = \sum_{p,q=0}^{\infty} c_{pq}(I_1 - 3)^p (I_2 - 3)^q \quad (13)$$

where

$$I_1 = \sum_{i=1}^{3} \lambda_i^2 \quad (14)$$

$$I_2 = \lambda_1^2\lambda_2^2 + \lambda_2^2\lambda_3^2 + \lambda_3^2\lambda_1^2 \quad (15)$$

$$I_3 = \lambda_1^2\lambda_2^2\lambda_3^2 = 1 \tag{16}$$

$c_{00} = 0$ so that zero deformation corresponds to zero strain energy. We have found that truncating the series at the third order terms is sufficient for our purposes. In terms of strain energy, the slip-tube model from eq 7 can be rewritten as

$$\frac{W_{ST}}{A} = \frac{1}{2}\sum_\alpha \left(\frac{\lambda_\alpha}{g_\alpha^{1/2}} + \frac{g_\alpha^{1/2}}{\lambda_\alpha}\right) - \frac{2}{3}\sum_\alpha \ln(g_\alpha^{1/2}) - 3 \tag{17}$$

This function also goes to $W = 0$ for $\{\lambda_\alpha\} = 1$.

For any given deformation, $\{g_\alpha\}$ can be calculated self-consistently from eqs 8−12 using the iterative secant method. With those $\{g_\alpha\}$, the strain energy can be calculated from eq 17. Repeating this procedure many times leads to a set of strain energies with their associated strain invariants. The entire data set can then be described using eq 13 by applying a nonlinear least-squares fit to determine the c_{pq} coefficients.

To generate the fitting data set, deformations corresponding to $0.3 \le \{\lambda_\alpha\} \le 3.0$ were used. This range was chosen as representative of the types of deformation encountered during standard O-ring usage. The deformations were chosen systematically by a double loop over λ_1 and λ_2 with $\lambda_3 = 1/(\lambda_1\lambda_2)$ and keeping only the points such that all three principal stretch ratios lie between 0.3 and 3.0.

Figure 1 compares the fit strain energies with the self-consistent calculations. When fitting to the strain energy determined by this map, the poorest fit was found for the small deformations. Thus, two fits (parameters shown in Table) were actually done for this data: one for $I_1 \le 5.0$ and $I_2 \le 6.27$ and one for the rest of the points. The errors in those fits are considerably less than 1%. Indeed, most of the range has an error of less than 0.1%. While larger strain invariants have larger error, the worst error seen is less than 2.5%. A point of concern was whether the artificiality of having two fits would cause anomalies in systems as they switch from one region to the other. Examining this region showed that anomalies are very small, with deviations only in the third significant figure.

To further compare the fit strain energy with the self-consistently calculated strain energy, calculations were done along a path corresponding to uniaxial extension. Uniaxial extension relates the three principal stretch ratios as

$$\lambda_1 = \lambda; \quad \lambda_2 = \lambda_3 = \frac{1}{\sqrt{\lambda}} \tag{18}$$

The comparison for this deformation mode is shown in Figure 2. Within the range of λ that was fit, the agreement is good, with less than 1% relative error between using the full strain energy and fit strain energy. As expected, the agreement rapidly deteriorates for deformations outside the fit region.

With an analytical form for the strain energy, the conversion to the calculation of the stresses from the principal stretch ratios is straightforward. The principal Cauchy stresses can be calculated from the strain energy by:

$$\sigma_{physical,\alpha} = \frac{\lambda_\alpha}{\det(\boldsymbol{\lambda})}\frac{\partial W}{\partial \lambda_\alpha} + p \tag{19}$$

where p is an indeterminate Lagrangian multiplier related to the hydrostatic pressure and determined by the specific deformation conditions. Using eqs 13 and 19 to calculate the principal stresses due to entanglements gives:

$$\frac{\sigma_{physical,\alpha}\det(\boldsymbol{\lambda})}{A} = 2\lambda_\alpha^2 c_{10} + 2\lambda_\alpha^2 c_{01}B + 2\lambda_\alpha^2 c_{11}[(I_2 - 3) + B(I_1 - 3)] + 4\lambda_\alpha^2 c_{20}(I_1 - 3) + 4\lambda_\alpha^2 c_{02}B(I_2 - 3) + 2\lambda_\alpha^2 c_{21}[2(I_1 - 3)(I_2 - 3) + B(I_1 - 3)^2] + 2\lambda_\alpha^2 c_{12}[2B(I_1 - 3)(I_2 - 3) + (I_2 - 3)^2] + 6\lambda_\alpha^2 c_{30}B(I_1 - 3)^2 + 6\lambda_\alpha^2 c_{03}B(I_2 - 3)^2 + p \tag{20}$$

where

$$B = \lambda_\beta^2 + \lambda_\gamma^2 \tag{21}$$

D. Total Cauchy Stress. As given in the previous sections, the stress from the chemical cross-links and physical entanglements includes a hydrostatic pressure through indeterminate Lagrangian multipliers. To make the stress fully determined, we subtract the hydrostatic component and then add the bulk modulus term to obtain

$$\boldsymbol{\sigma} = \sum_{i=1}^{n\,stages}\left\{\boldsymbol{\sigma}_{i,chemical} - \boldsymbol{I}\frac{Tr(\boldsymbol{\sigma}_{i,chemical})}{3} + \frac{G_i}{G}\kappa \ln\left[\frac{\det(\boldsymbol{\lambda})}{\det(\boldsymbol{\lambda}_i)}\right]\right\} + \boldsymbol{\sigma}_{physical} - \boldsymbol{I}\frac{Tr(\boldsymbol{\sigma}_{physical})}{3} + \frac{G_e}{G}\kappa \ln[\det(\boldsymbol{\lambda})] \tag{22}$$

G is the sum of the moduli for networks not at their state of ease, which includes the entanglement network if appropriate. Only one entanglement network is considered. Simulation shows that only the first chemical network formed traps entanglements; later stages do not trap entanglements.[13]

III. Results and Discussion

The constitutive equation as described in section II was implemented into the finite element code, Adagio.[17] Adagio is an implicit finite element code developed for quasistatic systems. Its strength lies in the multilevel solver that uses successive iterations to handle nonlinear material models and large deformations.

For validation of the constitutive model, two experimental studies, one in extension and one in compression, were chosen that had enough data to extract the cross-linking history from the stress relaxation data. Because only a single stress value was reported as a function of time, a uniform and uniaxial stress state is assumed. This assumption allows for a simple cube of material to be used as the geometry for the finite element calculations.

The necessary inputs to the theory are physical parameters and cross-linking/deformation history as a function of time. Because bulk modulus is infrequently reported for the exact materials used in these experiments, an estimation of the value must be made. The finite element calculations used a bulk modulus of 34.0×10^3 psi for all systems considered. This value was chosen based on previous experimental results obtained from similar materials that were tested at Sandia.

In order to estimate the cross-linking history, several assumptions were made. The important part of the history is what occurs after the deformation. Consequently, we need make no assumptions about how the first network is formed. It is sufficient to consider the first stage network fully formed before deformation and base its initial cross-link modulus, G_1*, on values obtained before significant network changes can occur. According to rubber elasticity theory,[20] the shear modulus of a single network can be related to initial cross-link density and entanglement density. In addition, the plateau modulus, G_N^0, can be used to estimate the entanglement modulus, G_e, using standard rubber elasticity theory. We have used these standard assumptions to make estimates for G_1* and G_e.

Extracting the instantaneous first and second cross-link density history from the experimental data is a bit more involved. In all cases, we have assumed first order kinetics for the scission

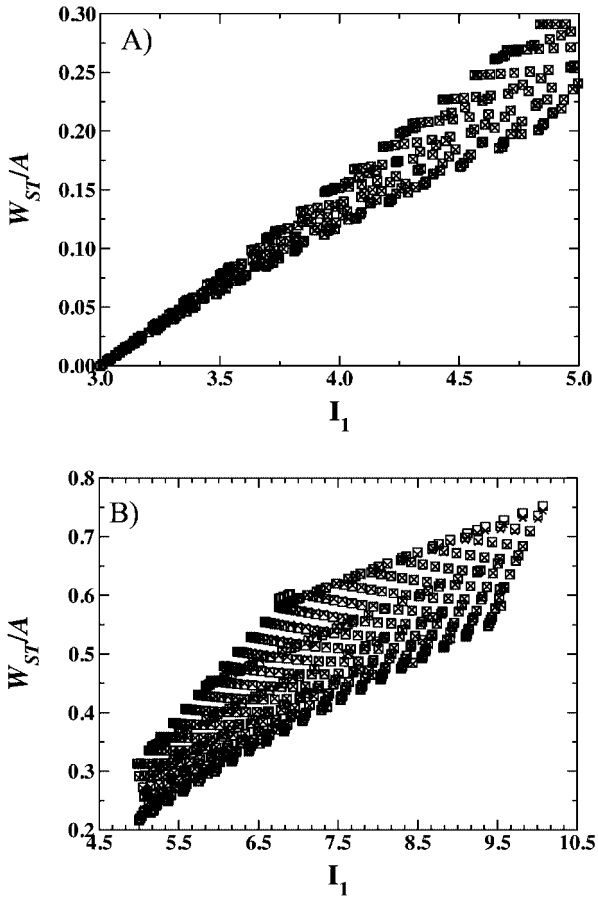

Figure 1. Strain energies from the slip-tube model. Comparison of self-consistent calculation and analytical fit. (A) For $I_1 \leq 5.0$ and $I_2 \leq 6.27$. (B) For the other deformations. Squares are the calculated strain energies from eq 17. The ×'s are from the fit to eq 13.

Table 1. Analytical Strain Energy Fits to the Slip-Tube Model Where Parameters Are Suitable for use in Eq 13

constant	$I_1 \leq 5.0$ and $I_2 \leq 6.27$	outside the small I range
c_{10}	0.0852	0.0944
c_{01}	0.0576	0.0434
c_{11}	−0.00335	0.00114
c_{20}	−0.00478	−0.00745
c_{02}	−0.00280	−0.000936
c_{21}	−0.000419	−0.000341
c_{12}	0.000503	0.0000767
c_{30}	0.000842	0.000553
c_{03}	0.000610	−0.0000339

reactions and have calculated rate constants for the first stage reactions by fitting the stress relaxation data from the experiments. However, estimating the second stage network formation is more complicated.

The obvious difficulty is that the second stage network does not have to form at a constant rate. Based on the necessity of aligning cross-linking units that have their mobility limited by prior network formation, it seems unlikely that the rate would be constant, particularly as possible reactants become separated by large distances.

The less obvious difficulty is that while the first network has a definite limit to the amount of scission that can occur, the second network may continue to form after the first network has been entirely eliminated. New cross-links formed after this point will not contribute to stress transfer. Chemically, no difference exists between a first and second stage cross-link. Thus, second stage cross-links also undergo scission, but they may reform. Memory of the original network fades as fewer cross-links were formed under its influence.

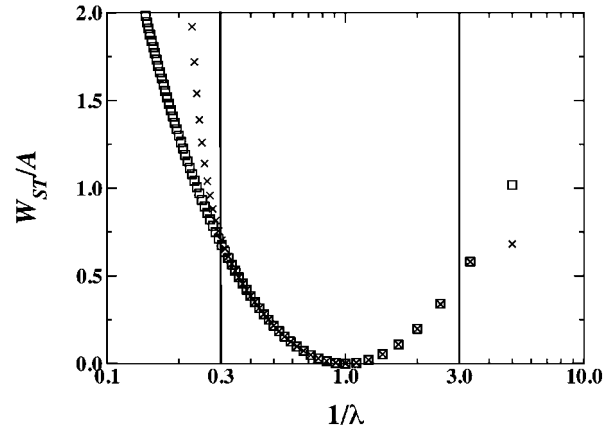

Figure 2. Strain energies from the slip-tube model. For uniaxial extension, comparison of analytical fit and self-consistent calculation. Squares are the calculated strain energies from eq 17. The ×'s are from the fit using eq 13.

To account for this situation when comparing with experiment, we have chosen to consider the second stage network as having two substages. The first substage, with modulus G_2^{α}, is comprised of cross-links that were formed while some portion of the stage one network existed and are thus able to act as effective stage one cross-links. The second substage, with modulus G_2^{β}, is comprised of cross-links that were formed after the stage one network dropped below the gel point and therefore should not be included in a calculation of G_1^{eff} because they cannot "come to the rescue" of the first network.

In the following sections, the details of extracting the cross-linking history from the stress data are given for each experimental study. The resulting cross-link history is shown for each study and finite element results are given for continuous stress relaxation. Then, permanent set is predicted using the chemical history data in the finite element calculations and is shown to be in good agreement with the experimental data.

A. Extension Comparison. The first experimental study is the classic butyl gum data from the Tobolsky group (Figure 7 of ref 5). Two different types of stress relaxation experiments were performed on samples from the same cure batch. Consequently, the chemistry of both samples as a function of time is expected to be the same. Both procedures report the ratio of current stress with initial stress for the time of the test. The main difference between the two types of investigation is their strain history. The resulting data from the two experiments give information about the total cross-link density and the effective stage one cross-link density as functions of time.

Continuous stress relaxation is the standard test during which the sample ages while held at a given strain and the resulting force is measured. This approach provides information about the effective stage one network as a function of time. In this case, the sample was uniaxially deformed to a stretch ratio of $\lambda_2 = 1.5$.

The less common experiment is intermittent stress relaxation. During the intermittent stress relaxation procedure, the sample is periodically stretched to λ_2 for long enough to take a stress reading and then the sample is released. As a result, the chemical reactions take place primarily in the unstretched state. The intermittent method provides information about the total cross-linking density of the sample. The data for butyl gum at 130 °C is shown in Figure 3.

By considering both sets of stress relaxation data, information about each network can be obtained. Considering the shape of the stress relaxation curves, we have broken the time into three periods based on the physical processes that are likely to be occurring. Because the stress decays quickly since the original

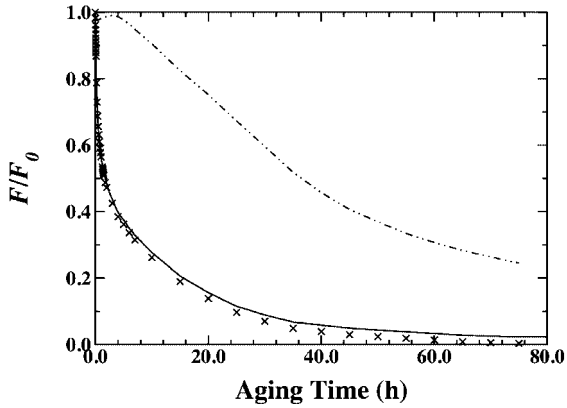

Figure 3. Stress relaxation of butyl gum. Comparison of experimental data from the Tobolsky group[5] and finite element calculations. The sample is butyl gum in uniaxial extension ($\lambda_2 = 1.5$) at 130 °C. The dashed line is intermittent stress relaxation data; the ×'s are continuous relaxation data. The solid line is finite element results using the fit parameters as described in the text.

network is completely eliminated very early, the effects of entanglements are small and have been neglected for this example.

At short time (less than 1.35 h), the near constant value of the intermittent stress relaxation means that the total cross-link density stays constant during that period so scission and cross-linking occur at equal rates. Under those conditions and the assumption of first order kinetics for scission, G_1 and G_2^{α} can be calculated as:

$$\frac{G_1^{eff}}{G_1^*} = \frac{1}{2 - \exp(-kt)}; \quad G_1 = G_1^* \exp(-kt);$$

$$G_2^{\alpha} = G_1^*(1 - \exp(-kt)) \quad (23)$$

Fitting the continuous stress relaxation data (which can be identified as G_1^{eff}/G_1^*) yields $k = 1.54\ \mathrm{h}^{-1}$.

At intermediate time, we assume that the first network continues to scission with first order kinetics; however, the second network no longer cross-links at the same rate. We calculate G_2^{α} after an aging time of 1.35 h using the continuous stress relaxation from the definitions of G_1^{eff} and Φ and solving for G_2^{α}. The resulting expression is

$$\frac{G_2^{\alpha}}{G_1^*} = \frac{\left[\frac{G_1^{eff}}{G_1^*} - \exp(-kt)\right]\left(1 + \frac{G_2^*}{G_1^*}\right)}{1 - \exp(-kt)} \quad (24)$$

G_2^* is the maximum in G_2^{α} up to the current time and is found through enforcing self-consistency. We ensure that the values of G_2^{α} obtained from first-order kinetics and eq 24 match at $t = 1.35$ h by adding an offset to the results of eq 24.

The third time period occurs as the original network drops below its gel point. Further changes in G_1^{eff} are now due to changes in G_2^{α} and therefore the continuous stress relaxation is primarily a measure of G_2^{α}. Again taking advantage of the fact that the intermittent stress relaxation is the sum of all cross-link contributions, G_2^{β} can be determined from:

$$\frac{G_2^{\beta}}{G_1^*} = \frac{F^{\mathrm{int}}}{F_0} - \frac{G_1}{G_1^*} - \frac{G_2^{\alpha}}{G_1^*} \quad (25)$$

where F^{int}/F_0 is the normalized intermittent stress relaxation.

The results for G_1, G_2^{α}, and G_2^{β} are shown in Figure 4 based on the shear modulus G having a value of 109 psi for the initial stage one modulus G_1^*. The peaks in both G_2^{α} and G_2^{β} are the result of scission occurring in the second stage cross-links.

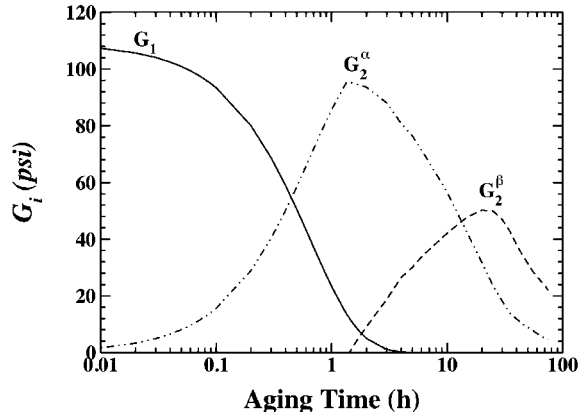

Figure 4. Cross-linking history deduced from the Tobolsky data.[5]

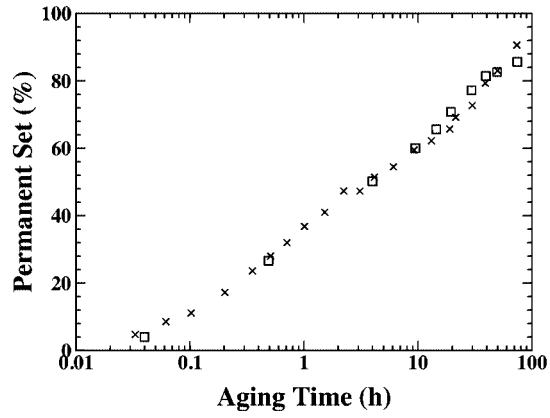

Figure 5. Permanent set comparison for finite element calculation and Tobolsky data.[5] Experimental data are denoted by ×'s and finite element calculations are squares.

Combining the chemistry and the elastic constants in the finite element calculation produces the continuous stress relaxation shown as a black curve in Figure 3. This is in excellent agreement with the experiment, as one would expect since, in essence, the parameters were fit for this data. This procedure verifies that the computer code for the model was correctly implemented.

A more stringent test is to predict permanent set. The finite element calculation was performed for the continuous stress relaxation test with restart files written at regular intervals. The finite element calculation for permanent set begins with one of the restart files. With the chemistry fixed for the network at that time, the sample was deformed back to the original shape. The stress was tracked during the deformation and the stretch ratio corresponding to the zero stress deformation was noted as λ_s. The permanent set can then be calculated from

$$PS = \frac{\lambda_s - 1}{\lambda_2 - 1} \times 100 \quad (26)$$

Figure 5 compares the finite element results with the experimental data. The agreement between our predictions and experiment is quantitative.

B. Compression Comparison. Gillen, Celina, and Bernstein[6] have reported sealing force relaxation data for butyl rubber O-rings from Burke Rubber Company (Compound 4061) at 125 °C. The data used was extracted from Figure 8 of ref 6. Times reported here are aging times to coincide with those reported in ref 6. The nominal deformation corresponds to $\lambda_2 = 0.75$. Unfortunately, only continuous stress relaxation data were reported so less information is available directly from experiment.

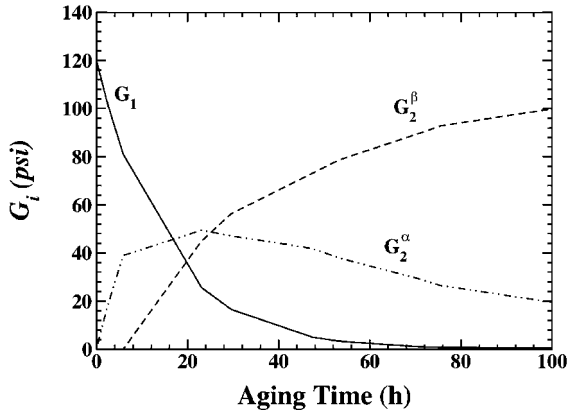

Figure 6. Cross-linking history for butyl O-ring.[6]

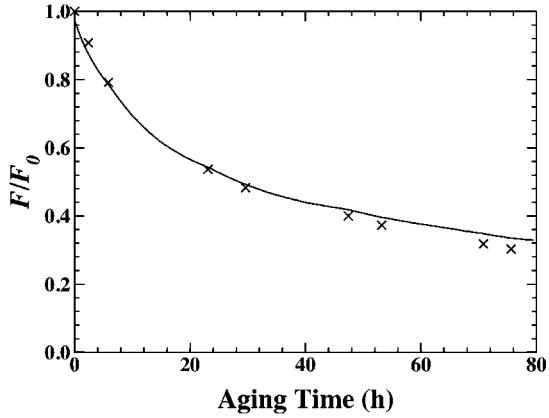

Figure 7. Continuous stress relaxation. Comparison of finite element calculations with experimental results from Gillen, Celina, and Bernstein.[6] Data is for O-ring from Burke Rubber Company (compound 4061) at 125 °C. Symbols are experiment; the line is the finite element calculation.

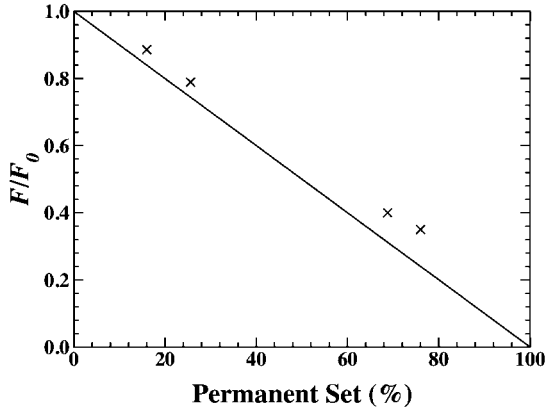

Figure 8. Permanent set for butyl rubber in compression. Symbols are from finite element calculation; line is derived from experiment as given in Gillen, Bernstein, and Wilson.[21]

Including the entanglement contribution slightly complicates the calculation of the cross-linking history from the stress relaxation. While the terms for the principal stretch ratios completely cancel for the chemical cross-links, the entanglement network retains a deformation dependency. The normalized continuous stress relaxation, F^{cont}/F_0, can be written as the ratio of the current stress to the initial stress just after deforming the sample. Writing the ratio in terms of the effective moduli gives

$$\frac{F^{cont}}{F_0} = \frac{G_1^{eff} + f(\lambda)G_e}{G_1^* + f(\lambda)G_e} = \frac{\dfrac{G_1^{eff}}{G_1^*} + \dfrac{f(\lambda)G_e}{G_1^*}}{1 + \dfrac{f(\lambda)G_e}{G_1^*}} \tag{27}$$

where $f(\lambda)$ is calculated from the uniaxial approximation to the slip-tube model[18] using

$$f(\lambda) = \frac{1}{0.74\lambda + \dfrac{0.61}{\sqrt{\lambda}} - 0.35} \tag{28}$$

Equation 27 can be written explicitly for G_1^{eff} as

$$\frac{G_1^{eff}}{G_1^*} = \frac{F^{cont}}{F_0} + \left[\frac{F^{cont}}{F_0} - 1\right]F_e \tag{29}$$

by defining the constant stress due to the entanglements as

$$F_e = \frac{f(\lambda)G_e}{G_1^*} \tag{30}$$

With less information, the time was only broken into two periods: before and after the original network had dropped below the gel point. Unfortunately, by 24 h the original network is below its gel point so only a few experimental data points are available for the initial time period.

Using eq 29, the effective stage one cross-links were determined for the time while the original network exists (up through time 5.86 h). By assuming first order kinetics with equal rates of cross-linking and scission applied (eq 23), a rate constant of $k = 0.067\ \text{h}^{-1}$ was determined and the applicable values of G_1 and G_2^α were calculated.

After time 5.86 h, it was assumed that equal rates of cross-linking and scission still hold so that G_2^β could be calculated from the total expected number of second stage cross-links by subtracting the value of G_2^α calculated from the stress relaxation function and G_1^{eff}. This will overestimate G_2^β since no provision is made for scission, even if the rate assumption is correct.

To determine numerical values for the moduli, estimates of the moduli for the original network were made from literature data. Graessley[20] reports a plateau modulus (G_N^0) of 32×10^4 Pa for polyisobutylene at 140 °C. Converting this for use in the slip-tube model[18] gives

$$G_e = \frac{4}{7}G_N^0\frac{T_{desired}}{T_{original}} = 26\ \text{psi} \tag{31}$$

making the simple assumption that the shear modulus G of 146 psi for polyisobutylene is merely the sum of the G_e and G_1^*, $G_1^* = 120$ psi.

The cross-link history determined for this sample is shown in Figure 6. The history is shown as continuous lines to show the linear interpolations between the values from the experimental data. The comparison of the calculated stress relaxation with experimental results is shown in Figure 7. As before, the agreement between calculated stress relaxation and experiment is good, further verifying the proper implementation of the model in the computer code.

Permanent set predictions were made using this cross-linking history in the finite element code. The same procedure to determine λ_s as described in the section on the extension experiment was used. As can be seen in Figure 8, the finite element predictions agree well with the experiment. Because of the assumption of equal rates of cross-linking and scission, the permanent set is likely to be too large at long time which corresponds to small stress and higher permanent set. This is observed in Figure 8 where the two small permanent set points

are closer to the experimental line than the two large permanent set points.

IV. Conclusion

The time-dependence of mechanical properties of rubber samples due to chemical aging is often neglected by constitutive models. We have addressed this knowledge gap by proposing a constitutive model developed from simulations. This model includes the effects of cross-linking and scission of polymer networks in deformed states. On the basis of the independent network hypothesis, this model also includes the effects of entanglements through the slip-tube model and the strain history memory by using a stress transfer function to evaluate effective networks. While most of the theories behind the constitutive model are not new, the model is the first to combine these ideas into a practical set of constitutive equations.

This new constitutive model was implemented into the Sandia proprietary finite element code, Adagio, and calculations were performed to compare with experimental data in both extension and compression. Using the chemistry extracted from experiment, the time-dependent stress from the calculations matched that of experiment. The permanent set predicted by the model was in good agreement with the experimental results.

The focus of this constitutive model was the physics of network formation and scission in deformed states on the mechanical properties of the samples. To enable completely predictive models, the chemistry of the reacting material should be included directly from simulation or separate experiment. Future work on this model will include efforts to predict the chemistry from simulation.

Acknowledgment. Sandia is a multiprogram laboratory operated by Sandia Corporation, a Lockheed Martin Company, for the United States Department of Energy's National Nuclear Security Administration under Contract DE-AC04-94AL85000.

References and Notes

(1) One particularly interesting long term study is: Brown, R. P.; Butler, T. *Natural Ageing of Rubber: Changes in Physical Properties over 40 Years*; Rapra Technology Limited: Shawbury, Shropshire, U.K., 2000.
(2) Curro, J. G.; Salazar, E. A. *Rubber Chem. Technol.* **1973**, *46*, 530.
(3) Curro, J. G.; Salazar, E. A. *J. Appl. Polym. Sci.* **1975**, *19*, 2571.
(4) Salazar, E. A.; Curro, J. G.; Gillen, K. T. *J. Appl. Polym. Sci.* **1977**, *21*, 1597.
(5) Andrews, R. D.; Tobolsky, A. V.; Hanson, E. E. *J. Appl. Phys.* **1946**, *17*, 352.
(6) Gillen, K. T.; Celina, M.; Bernstein, R. *Polym. Degrad. Stab.* **2003**, *82*, 25.
(7) Wineman, A. S.; Rajagopal, K. R. *Arch. Mech.* **1990**, *42*, 53.
(8) Shaw, J. A.; Jones, A. S.; Wineman, A. S. *J. Mech. Phys. Solids* **2005**, *53*, 2758.
(9) Jones, A. An Experimental Study of the Thermo-Mechanical Response of Elastomers Undergoing Scission and Crosslinking at High Temperatures, Ph.D. Dissertation, University of Michigan, **2003**.
(10) Septanika, E. G.; Ernst, L. J. *Mech. Mater* **1998**, *30*, 253. (b) Septanika, E. G.; Ernst, L. J. *Mech. Mater.* **1998**, *30*, 265.
(11) Flory, P. J. *Chem. Rev.* **1944**, *35*, 51.
(12) Flory, P. J. *Proc. Natl. Acad. Sci. U.S.A.* **1960**, *56*, 722.
(13) Rottach, D. R.; Curro, J. G.; Grest, G. S.; Thompson, A. P. *Macromolecules* **2004**, *37*, 5468.
(14) Rottach, D. R.; Curro, J. G.; Budzien, J.; Grest, G. S.; Svaneborg, C.; Everaers, R. *Macromolecules* **2006**, *39*, 5521.
(15) Rottach, D. R.; Curro, J. G.; Budzien, J.; Grest, G. S.; Svaneborg, C.; Everaers, R. *Macromolecules* **2007**, *40*, 131.
(16) Fricker, H. S. *Proc. R. Soc. London, Ser. A Math. Phys. Sci.* **1973**, *335*, 267.
(17) SIERRA Solid Mechanics Team "Adagio 2.9 User's Guide" Sandia National Laboratories; SAND2008−2976.
(18) Rubinstein, M.; Panyukov, S. *Macromolecules* **2002**, *35*, 6670.
(19) Treloar, L. R. G. *The Physics of Rubber Elasticity*, 2nd ed.; Oxford University Press: London, 1958; p 155.
(20) Graessley, W. W. *Polymeric Liquids and Networks: Structure and Properties;* Garland Science: New York, 2004; p 454.
(21) Gillen, K. T.; Bernstein, R.; Wilson, M. H. *Polym. Degrad. Stab.* **2005**, *87*, 257.

MA801373Z